Fatigue Crack Growth in EUROFER 97 at Different Temperatures

J. Aktaa, M. Lerch

Institut für Materialforschung
Programm Kernfusion
Association Forschungszentrum Karlsruhe/EURATOM

Mai 2005

Abstract

For the assessment of cracks in First Wall structures built from EUROFER 97 of future fusion reactors the fatigue crack behaviour in EUROFER 97 was investigated at room temperature (RT), 300, 500 and 550°C. For this purpose fatigue crack growth tests were performed using CT specimens with two R-ratios, $R = 0.1$ and $R = 0.5$, respectively. Hence, fatigue crack threshold, fatigue crack growth behaviour in the near-threshold range and their dependences on temperature and R-ratio were determined and described using an analytical formula. The fatigue crack threshold showed a monotonic dependence on temperature which is for $R = 0.5$ insignificantly small. The fatigue crack growth behaviour exhibited for $R = 0.1$ a non-monotonic dependence on temperature which is explained by the decrease of yield stress and the increase of creep damage when increasing the temperature.

Ermüdungsrisswachstum in EUROFER 97 bei verschiedenen Temperaturen

Zusammenfassung

Zur Beurteilung von Rissen in aus EUROFER 97 gefertigten Strukturen der Ersten Wand zukünftiger Fusionsreaktoren wurde das Ermüdungsrissverhalten in EUROFER 97 bei Raumtemperatur (RT), 300, 500 und 550°C untersucht. Hierfür wurden bei jeder Temperatur Ermüdungsrissexperimente an CT-Proben mit zwei unterschiedlichen R-Verhältnissen, $R = 0.1$ und $R = 0.5$ durchgeführt. Daraus wurden der Ermüdungsrisswiderstand und das Ermüdungsrissverhalten im risswiderstandsnahen Bereich sowie ihre Abhängigkeiten von der Temperatur und dem R-Verhältnis ermittelt und mit analytischen Formeln beschrieben. Der Ermüdungsrisswiderstand zeigte eine monotone Abhängigkeit von der Temperatur, die bei $R = 0.5$ geringfügig ist. Das Ermüdungsrissverhalten hingegen wies bei $R = 0.1$ eine nicht-monotone Abhängigkeit von der Temperatur auf, die auf die Abnahme der Fließspannung und die Zunahme der Kriechschädigung mit steigender Temperatur zurückgeführt wird.

Contents

1 Introduction

EUROFER 97 as reduced activation ferritic martensitic (RAFM) steel, developed recently inter alia in the framework of EURATOM Fusion Technology programme, is potential candidate for structural materials of future fusion reactors [1]. During planed operation of a fusion reactor structural materials of the plasma facing components, Blanket and Divertor, are subjected to cyclic thermo-mechanical loading and high irradiation doses which induce different kinds of damage: creep, fatigue as well as irradiation damage [2]. For the assessment of cracks initiated in Blanket or Divertor components due to this damage and detected during non-destructive inspection fracture mechanical data, among others data describing crack behaviour under fatigue (cyclic) loading are necessary. Therefore within our activities in the EFDA Technology Work programme with the reference TTMS-002 "Metallurgical and Mechanical Characterisation" fatigue crack growth in EUROFER 97 at different temperatures was investigated. Fatigue crack growth experiments were performed at RT, 300, 500 and 550°C using CT specimens. Crack threshold and crack growth rate as well as their dependence on temperature and R-ratio (minimum load divided by maximum load within a cycle) were determined.

In the following the procedures after which the fatigue crack growth experiments were conducted and evaluated are described. Thereafter the main results are presented and discussed.

2   Experimental

2.1   Material and specimen geometry

The fatigue crack growth experiments were performed on the ferritic-martensitic steel EU-ROFER 97 in the as delivered state. The specimens were cut from the semi-finished product fabricated by Böhler Edelstahl GmbH, Austria [3]. Manufacturing of the batches is described by the manufacturer in [4]. Chemical compositions of the batches according to the analysis certificates are listed in Table 1.

The specimens were cut off from a plate of 490 mm x 116 mm x 25 mm in size. Specimen dimensions corresponded to the ASTM standard E 647-95a for the determination of the K_{IC} value. They were taken with their length parallel to the rolling direction (WR). Figure 1 shows the specimen geometry with all dimensions and surface characteristics being indicated.

Prior to the start of the test, a fatigue crack is generated starting from the crack-starter notch using a frequency of 30 Hertz being the same as during the test. The total length of the initial crack is adjusted to be 17 mm measured from the load line. During the test, the crack reaches a length of more than ½ W (W is distance between the load line and specimen edge) [5]. When generating the initial crack, maximum load is chosen such that the following estimated stress intensity is not exceeded at the end of initial cracking:

$$\frac{K_{\max}}{E} \leq 3.2 \times 10^{-4} \sqrt{m} \qquad (2.1)$$

To measure the crack extension during the test the electric potential method described bellow is used. For applying this method a constant current is passed in the specimen by plugs attached to two M5 tapped holes of 10 mm depth located in the centre of the upper and lower side of the specimen. To measure the potential two M3 tapped holes of 6 mm depth are added at a distance of 5 mm above and bellow the front of the initial crack and for symmetry reasons on both sides of the specimen, respectively, (s. Figure 1). In this way, it is ensured that the contact points for potential measurement are very close to the crack which makes the measurement sufficiently sensitive to crack extension.

2.2   Electric potential method (DC)

The principle of this method is based on passing in the specimen a current that is constant with time. Since crack extension results in reduction of the remaining ligament an increase of the voltage U is necessary for keeping the current constant. Thus the voltage increase $\Delta U = U - U_0$ can be correlated with the crack extension $\Delta a = a - a_0$. For monitoring the voltage the difference in the electric potential of two points located equidistant above and below the remaining ligament is measured. The positions of these points shall be selected so that the potential difference becomes sensitive to crack extensions and at the same time its measurement can be carried out without significant influence on loading flow. For the correlation between voltage change and crack extension Johnson [6] has derived an analytic for-

mula for flat specimen with center crack which was found to be applicable on CT specimen [7]. According to this formula the crack length can be determined as

$$a = \frac{2W}{\pi} \arccos\left(\frac{\cosh\left(\dfrac{\pi y}{2W}\right)}{\cosh\left[\dfrac{U}{U_0} ar\cosh\left(\dfrac{\cosh\left(\dfrac{\pi y}{2W}\right)}{\cosh\left(\dfrac{\pi a_0}{2W}\right)} \right) \right]} \right) \tag{2.2}$$

with

a crack length

a_0 initial crack length

W distance between load line and specimen edge

y half of the distance between the potential measurement points

U potential difference (voltage)

U_0 initial potential difference (voltage)

Applying the electric potential method to our CT specimen current generated by a DC supplier unit of Heinzinger Co. and FUG is passed in the specimen via cables screwed to the M5 tapped holes. The potential difference (voltage) is measured between the M3 tapped holes by screwing wires connected to a nano-voltmeter, type 181, made by Keithley. In the temperature range up to 300°C 6 mm^2 and 1.5 mm^2 copper wires are used for the current supply and voltage tapping, respectively. The wires are connected to the specimens using stainless steel screws and are insulated from the specimen holder by ceramic tubes. At 500 and 550°C the copper wires have to be replaced by Kanthal or Thermanit wires [8], as they are subject to strong oxidation at the surface and contact points and due to the measurement signal becomes unsteady and is no longer suited for a correlation with the crack length.

In preliminary tests the change in crack length determined using Johnson's relation (eq. 2.2) is compared to the values measured by fractography and thereby good agreement is observed. In addition to the calculated crack length, all specimens are cracked up after the crack stop, and the end crack length is measured.

As the conductivity of the wires changes strongly due to the high temperatures, the absolute voltage values measured differ considerably from those at room temperature. Moreover, varying wires, screws, washers, and cross sections cause the voltage to change. The ratio U/U_0, however, remains the same at all temperatures, such that Johnson's formula can always be applied.

2.3 Experimental setup

The tests were performed using a Schenk servo-hydraulic testing machine with a load capacity of 63 kN. The testing machine is controlled by an Instron controller of the series 8500. For mounting the specimen fork-shaped specimen holders connected to the rods of the machine are used whereas the specimen is fixed using two adapted bolts. Load parameters, amplitude, mean value and frequency are input directly via the Instron operation board.

For high temperatures tests, a 3-zone furnace with a heating power of 5 KW is used. The furnace is fixed to the frame of the testing machine and encloses the specimen. The zones can be controlled separately by the Jumo PID controllers. Thus, the temperature required can be maintained homogeneously distributed. The temperatures controlled are measured by Ni-NiCo thermocouples that are attached to the specimen holder and the specimen itself. In addition a Ni-NiCo thermocouple for monitoring the specimen temperature is fixed to the wide front side of the specimen by welded small sheet metal plates. The thermocouple is arranged close to the crack but such that it is not reached by the crack during the test.

For data acquisition an external PC with DASYLAB - data acquisition ware – is used. This PC records the test data needed and stores them. It is connected to the Instron control system of the testing machine to collect the values for mean and maximum load. These data only serve for control purposes so as to ensure that the load and its amplitude are kept constant. Particular attention is paid to potential measurement data collected from the nano-voltmeter which are used to calculate the crack length and in addition to generate a trigger signal for stopping the testing machine when the crack has reached a certain length.

2.4 Experimental procedure

After mounting the specimen in the testing machine an initial crack is created as described in section 2.1. To monitor the initial crack, crack length is checked constantly using a light microscope. As a light source, a stroboscope lamp is used. Its flashing signal can be set such that its frequency is close to loading frequency. In this way, the observer watches the closing and opening of the crack in slow motion and may pursue crack propagation. For a better marking of the crack, the crack and the area around it are blackened by a felt-tipped pencil. As soon as the initial crack has reached its desired length, it is stopped by turning-off the loading. Hence, the specimen is ready for the test.

Before starting the test the wires of the electric potential measuring system are connected to the specimen. Then, in the case of high temperature test, the specimen is heated under load control up to the test temperature. The test is started applying a sinusoidal load with a frequency of 30 Hz, a load range ΔF and a mean load F_{mean} determined by the R-Ratio of the test R and a ΔK value leading to a remarkable crack growth rate

$$\Delta K = \frac{\Delta F}{B\sqrt{W}} * \frac{\left(2 + \frac{a}{W}\right) * \left(0.886 + 4.64\frac{a}{W} - 13.32\left(\frac{a}{W}\right)^2 + 14.72\left(\frac{a}{W}\right)^3 - 5.6\left(\frac{a}{W}\right)^4\right)}{\left(1 - \frac{a}{W}\right)^{3/2}} \qquad (2.3)$$

$$F_{mean} = \frac{\Delta F}{2} \left(\frac{1+R}{1-R} \right) \qquad\qquad (2.4)$$

with B as the specimen thickness. After a certain amount of crack extension determined by a predefined increase in the voltage monitored ΔK and accordingly ΔF and F_{mean} are reduced in steps whereas the initial reduction is the largest, as the crack growth rate is significantly high. With decreasing crack growth rate, the increment is decreased as well to prevent a crack stop by the preceding plastic zone. In each step a predefined increase in the voltage and thus a crack extension of approximately the same amount is bided. This stepwise reduction of crack loading is continued until the crack is stopped. Under the last cyclic load after a million load cycles, no crack change should be measured. Only then is the test completed. In the meantime, the recorded potential data are stored in an Excel table with the load and test parameters being indicated.

Upon the completion of the test, the specimen is subjected to cyclic loading until it breaks. The ΔK value is the same as during initial cracking. In the tests at room temperature, the specimen is subjected to prior heating to a temperature of 300°C for 3 hours to mark the crack front. After the high-temperature tests, the specimen is not heated again, but broken in the cooled state at room temperature. The crack length of the damaged specimen is measured at 3 points at distances of $B/4$ each. The average value from the measurements is compared to the value determined by the electric potential measurements.

3   Tests and evaluation

Fatigue crack growth tests were performed with EUROFER 97 CT specimens at RT, 300, 500 and 550°C, respectively. At each temperature the influence of R-ratio was investigated performing two experiments with $R = 0.1$ and $R = 0.5$, respectively. The aim of the experiments is the determination of fatigue crack threshold ΔK_{th}, the relation between fatigue crack growth rate da/dN and crack loading ΔK, and their dependence on temperature and R-ratio as well.

The data acquisition during a test delivers for the different loading steps the crack length versus number of cycles. Plotting these values for each step a common behaviour can be recognized. At the beginning of the step the crack starts growing with a relatively low rate which increases successively with increasing crack length. The low rate at the beginning can be explained by the fact that the crack needs to overcome the plastic zone in the front of the crack tip induced in the previous step with a loading higher than the current one. Thereafter the crack growth with be accelerated by increasing crack loading (ΔK) with increasing crack length (a). However, da/dN and ΔK are actually not constant during one step, and mean representative values have to be determined. Therefore two methods were analyzed. With the first one a polynomial of 3rd order is fitted to the crack length versus number of cycles values measured within a step. The polynomial is then used to determine da/dN and ΔK versus number of cycles and thereof the mean values of the step. With the second method the mean value of the crack growth rate is determined - according to the widely used secant

method [9] - simply by the crack growth increment Δa measured within a step divided by the number of cycles of the step ΔN. The mean value of ΔK is determined as the average of its values at the beginning and at the end of the step. Since the results of the second method were more conservative than those of the first more accurate method we decided to proceed with the evaluation using the second method.

The mean values for da/dN and ΔK determined for all steps of a test are then plotted in a da/dN - ΔK -diagram and described by fitting the following relation

$$\frac{da}{dN} = A\left(\Delta K^n - \Delta K_{th}^n\right) \tag{3.1}$$

with A and n as material, temperature and R-ratio dependent parameters. Before performing the fit the fatigue crack threshold ΔK_{th} - which is also material, temperature and R-ratio dependent - is identified as the mean value of the minimum ΔK with fatigue crack growth and the next lower value with no fatigue crack growth. A and n are determined by least square fit of the relation 3.1 to the experimental values.

4   Results and discussion

Figure 2 and Figure 3 show the da/dN vs. ΔK curves obtained form the tests performed at different temperatures with $R = 0.1$ and $R = 0.5$. The markers represent the experimental values and the solid lines their description fitting eq. 3.1 whereas the values determined thereby for A and n are listed with the values for ΔK_{th} in Table 2.

On Figure 2 it can be recognized that for $R = 0.1$ the fatigue crack threshold ΔK_{th} as expected decreases when increasing the temperature whereas the fatigue crack rate at higher ΔK values shows a non-monotonic dependence on the temperature with the lowest value at 300°C and the highest value at 550°C. The low value at 300°C can be explained by stronger crack tip blunting due to decreased yield stress in comparison to that at RT. At 500 and 550°C creep and oxidation become significant yielding to higher crack growth rate.

For $R = 0.5$, s. Figure 3, a non-monotonic dependence on the temperature of the fatigue crack rate at ΔK values higher than the fatigue crack threshold has not been observed. In addition the dependence on the temperature is not as high as it is for $R = 0.1$. Also the fatigue crack threshold depends insignificantly on the temperature.

The values of ΔK_{th} obtained for room temperature (RT) and different R-ratio, s. Table 2, fit fairly well in the range identified by Liaw et al. for Fe alloys at RT [10]. In addition the values determined for the exponent n (s. Table 2) at RT and 300°C correspond well with the value of 2 cited in the literature [11]. However the values of n at 500 and 550°C are much lower which implies a lower increase of the crack growth rate when increasing ΔK. This might be explained by the fact that at these temperatures inelastic deformation particularly creep consumes a significant part of the increase in the deformation energy when increasing ΔK and accordingly the increase of the crack driving force and crack growth rate are lower.

The investigations by light microscopy and scanning electron microscopy (SEM) clearly show the temperature influence on the specimens. Along the entire crack, the surface of the crack exhibits a thick oxide layer (s. Figure 4). Only in the area of about 20 µm behind the crack tip does the thickness of the oxide layer decrease. However, it still extends to the crack tip in a thinner layer. The entire surface is covered densely, such that the structure of the crack pattern is not visible in the high-temperature specimens. It may be assumed that oxidation during crack growth extends up to the crack tip, where it influences the crack propagation behaviour. With decreasing crack rates due to the smaller load amplitudes, the oxidation processes gain importance as far as the slip activities close to the crack tip are concerned.

The etched grindings of the lateral surface of the crack reveal the crack behaviour in the microstructure. It is clearly visible how the crack intersects the grains in a transcrystalline manner and eventually stops at the grain boundary (s. Figure 5). In no area of the crack length can an intercrystalline geometry of the crack be seen. Even the crack start is transcrystalline. Hence, it is clear that the pile-up of dislocations at grain boundaries and the associated increase in the stress are not sufficient to break up the grain boundaries. Crack resistance inside the grains always is smaller than at the grain boundaries, even in the high-temperature tests. Consequently, it may be assumed that EUROFER 97 tends to crack in a transcrystalline manner under the load amplitudes applied.

5   Literature

[1]   B. van der Schaaf, F. Tavassoli, C. Fazio, E. Rigal, E. Diegele, R. Lindau and G. Le-Marois, "The development of EUROFER reduced activation steel," Fusion Engineering and Design, Volume 69, Issues 1-4, September 2003, Pages 197-203.

[2]   E. Diegele, D. Munz and G. Rizzi, "Design and life assessment of first wall components," Fusion Engineering and Design, Volume 27, 1 March 1995, Pages 210-215.

[3]   M. Schirra, A. Falkenstein, P. Graf, S. Herger, H. Kempe, R. Lindau, H. Zimmermann, "Ergebnisse von Charakterisierungsuntersuchungen zu physikalischen und mechanischen Eigenschaften des martensitischen 9% Cr-Stahls EUROFER 97," FZKA 6707, 2002

[4]   R. Schneider, P. Würzinger, G. Lichtenegger, H. Schweiger, "Metallurgie an den Grenzen höchster Reinheitsgrade und niedrigster Spurenelementgehalte," BHM 145, 2000, Heft 5, S. 199-203

[5]   Klaus Heckel, "Einführung in die technische Anwendung der Bruchmechanik," Hanser Studien Bücher, 1970.

[6]   H.H. Johnson, "Calibrating the Electric Potential Method to Studying Slow Crack Growth," Materials Research & Standards, 1965, pp. 442-445.

[7]   K.H. Schwalbe, "Bruchmechanik metallischer Werkstoffe," Carl Hanser Verlag, 1980.

[8]   H. Lange, "Rissausbreitung im Stahl AISI 316 L bei erhöhter Temperatur unter stati-
        scher und zyklischer Belastung," KFK 4823, 1991.

[9]   A. Saxena and Ch. L. Muhlstein, "Fatigue crack growth testing," ASM Handbook, Vol.
        19: Fatigue and Fracture, pp. 168-181.

[10]   P. K. Liaw, T.R. Leax & W. A. Logsdon, "Near-threshold fatigue crack growth behavior
        in metals," Acta Metallurgica 31(1983)1581-1587.

[11]   A.E. Carden, "Parametric analysis of fatigue crack growth," paper C324/73, in Interna-
        tional Conference on Creep and Fatigue in Elevated Temperature Applications,
        ASME, 1973.

Appendix A Tables and Figures

Table 1: Chemical composition of EUROFER 97

	Specifications in %	Manufacturer's analysis of batch 83699/83698 in %	IMF analysis of batch 83698 in %
Cr	8.50-9.50	8.87/8.82	9.21
C	0.09-0.12	0.12/0.11	0.104
Mn	0.20-0.60	0.42/0.47	0.502
V	0.15-0.25	0.19/0.20	0.204
W	1.00-1.20	1.10/1.09	1.148
Ta	0.05-0.09	0.14/0.13	0.14
N_2	0.015-0.045	0.018/0.020	0.0234
O_2	max. 0.01	0.0013/0.0010	<0.001
P	max. 0.005	0.004/0.005	<0.04
S	max. 0.005	0.003/0.004	0.004
B	max. 0.001	<0.0005/0.001	<0.01
Ti	max. 0.01	0.008/0.005	0.004
Nb	max. 0.001	<0.0010/0.0016	12 ppm
Mo	max. 0.005	<0.0010/0.0010	<8
Ni	max. 0.005	<0.0070/0.0200	214
Cu	max. 0.005	0.022/0.0016	35
Al	max. 0.01	0.008/0.009	51
Si	max. 0.05	0.07/0.04	430
Co	max. 0.005	0.004/0.006	67
As+Sn+Sb+Zr	max. 0.05	<0.015/0.015	
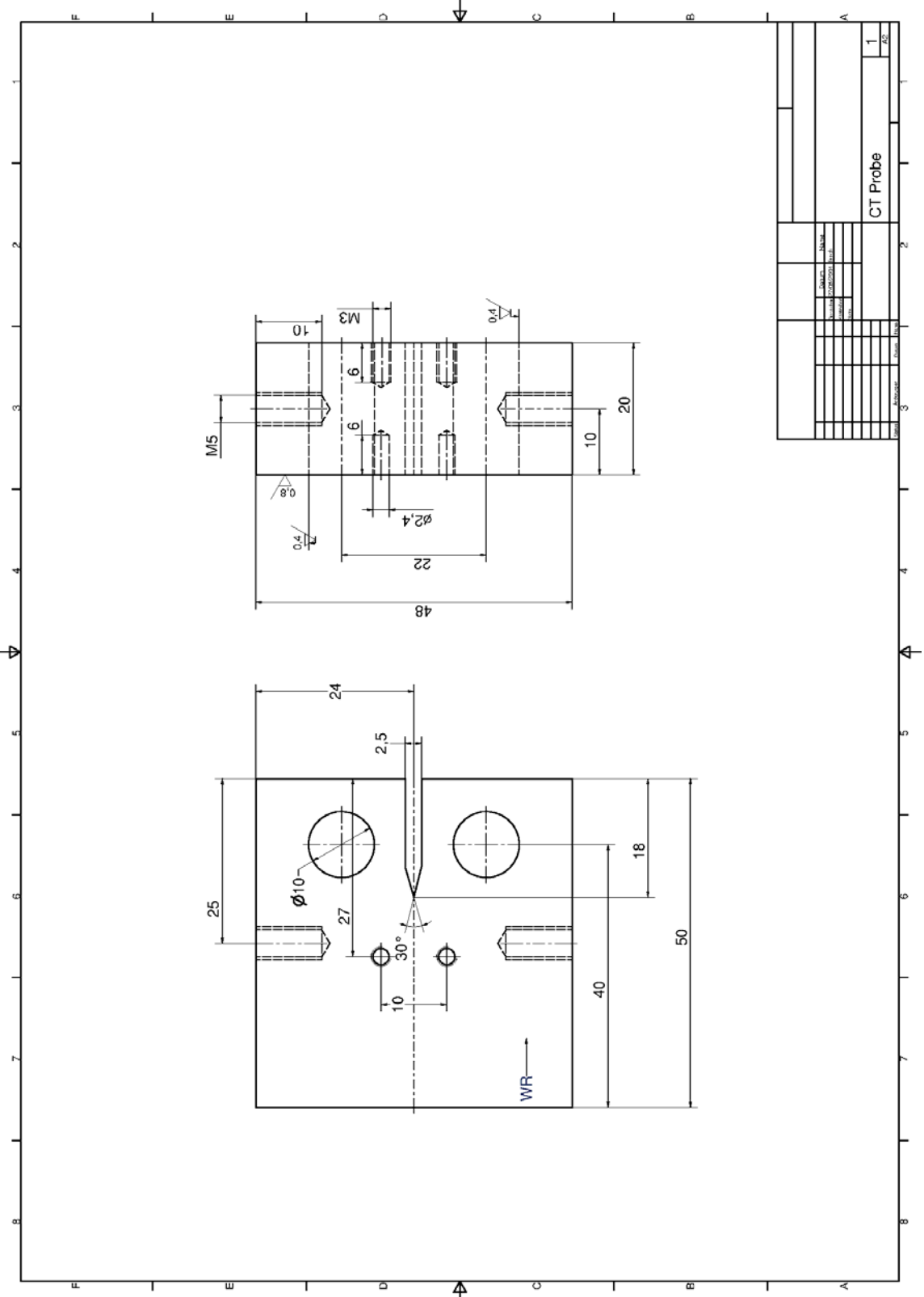
Figure 1   Engineering detail drawing of the CT specimen used
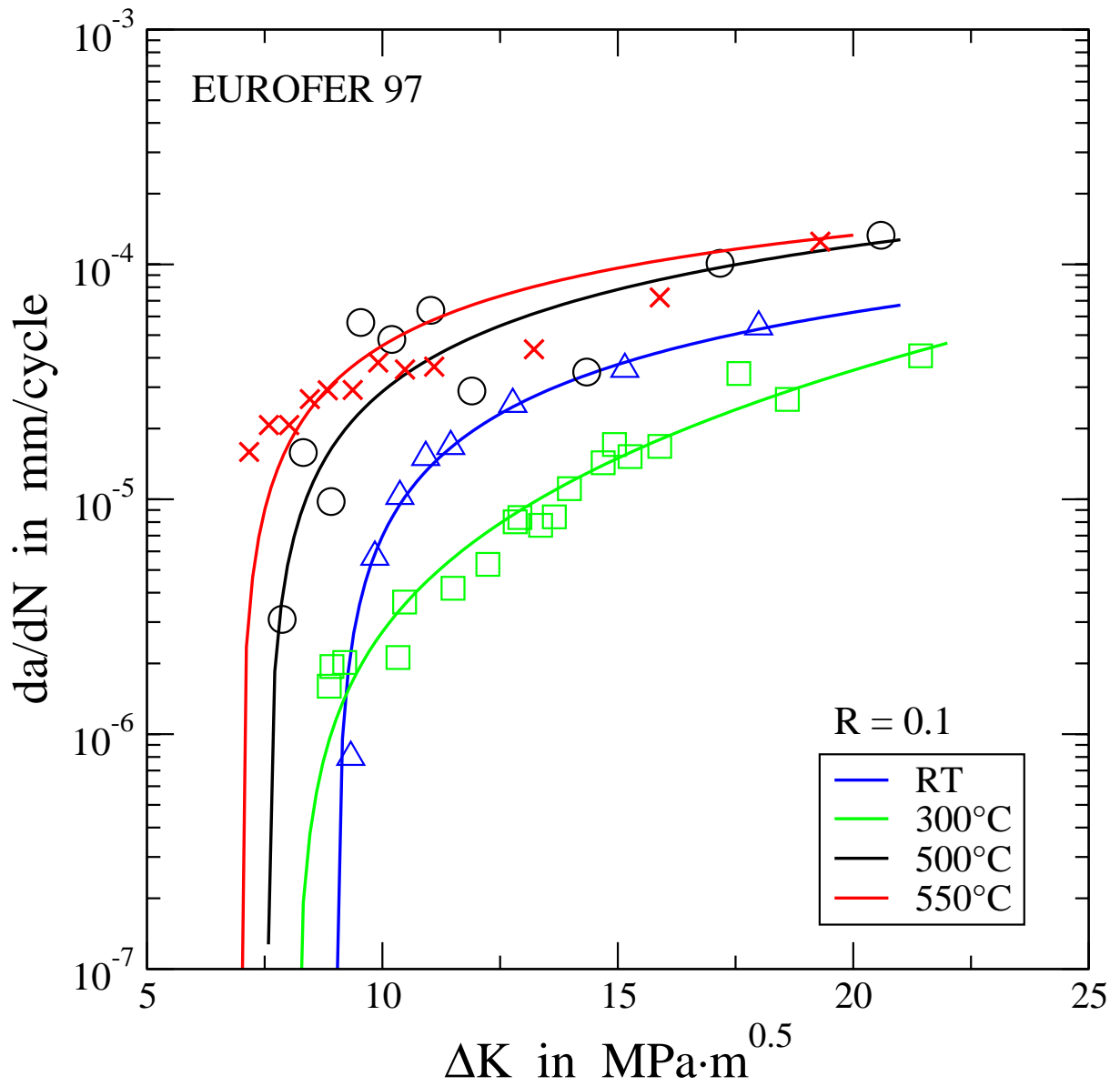
Figure 2   *da / dN* vs. *ΔK* behaviour at different temperatures in comparison for *R* = 0.1
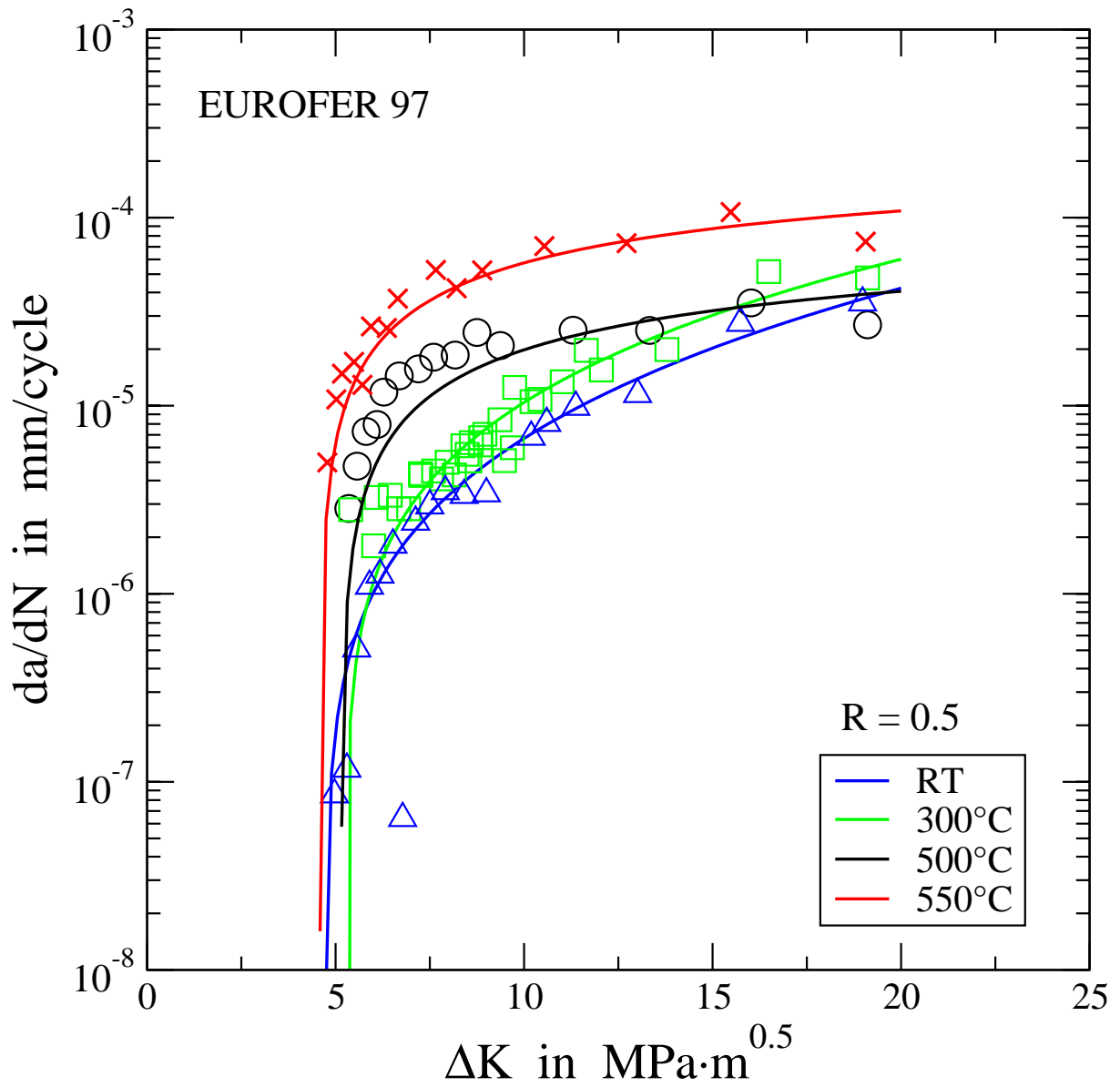
Figure 3   *da / dN* vs. ΔK behaviour at different temperatures in comparison for $R = 0.5$

Tabelle 2   Values determined for ΔK_{th}, A and n (eq. 3.1)

R-ratio	Temperature °C	ΔK_{th} MPa$\cdot\sqrt{m}$	A mm/cycle/$\left(MPa\cdot\sqrt{m}\right)^n$	n
0.1	RT	9.02	6.16×10^{-5}	0.423
	300	7.84	1.95×10^{-8}	2.541
	500	7.57	7.44×10^{-5}	0.485
	550	6.98	4.37×10^{-3}	0.027
0.5	RT	4.73	2.86×10^{-8}	2.445
	300	5.23	8.42×10^{-8}	2.211
	500	5.15	3.67×10^{-3}	7.97×10^{-3}
	550	4.59	5.21×10^{-1}	1.413×10^{-4}
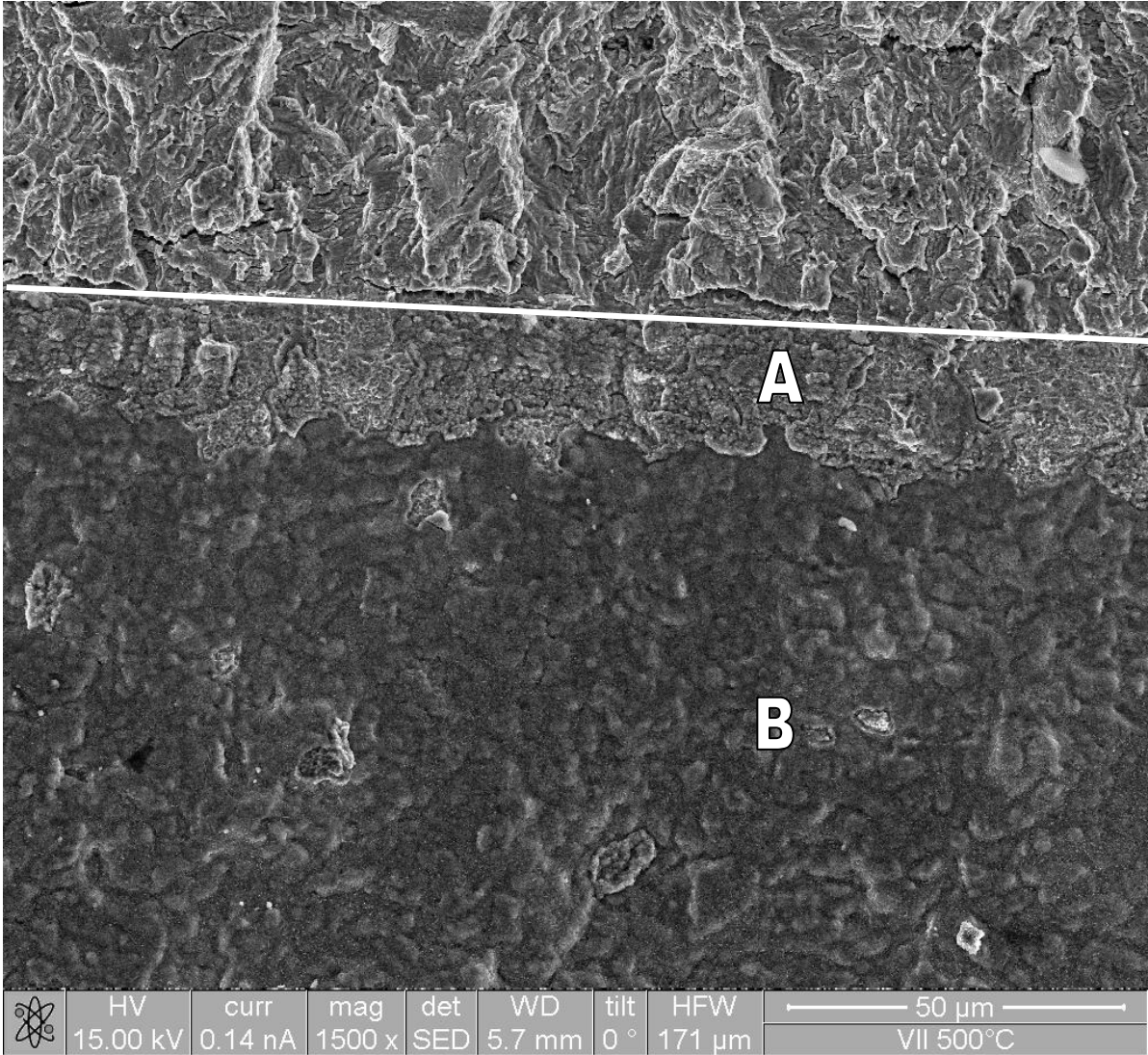
Figure 4   SEM Crack surface with oxide layer. The white line marks the crack front, A and B mark the areas with thin and thick oxide layer, respectively.

20 µm
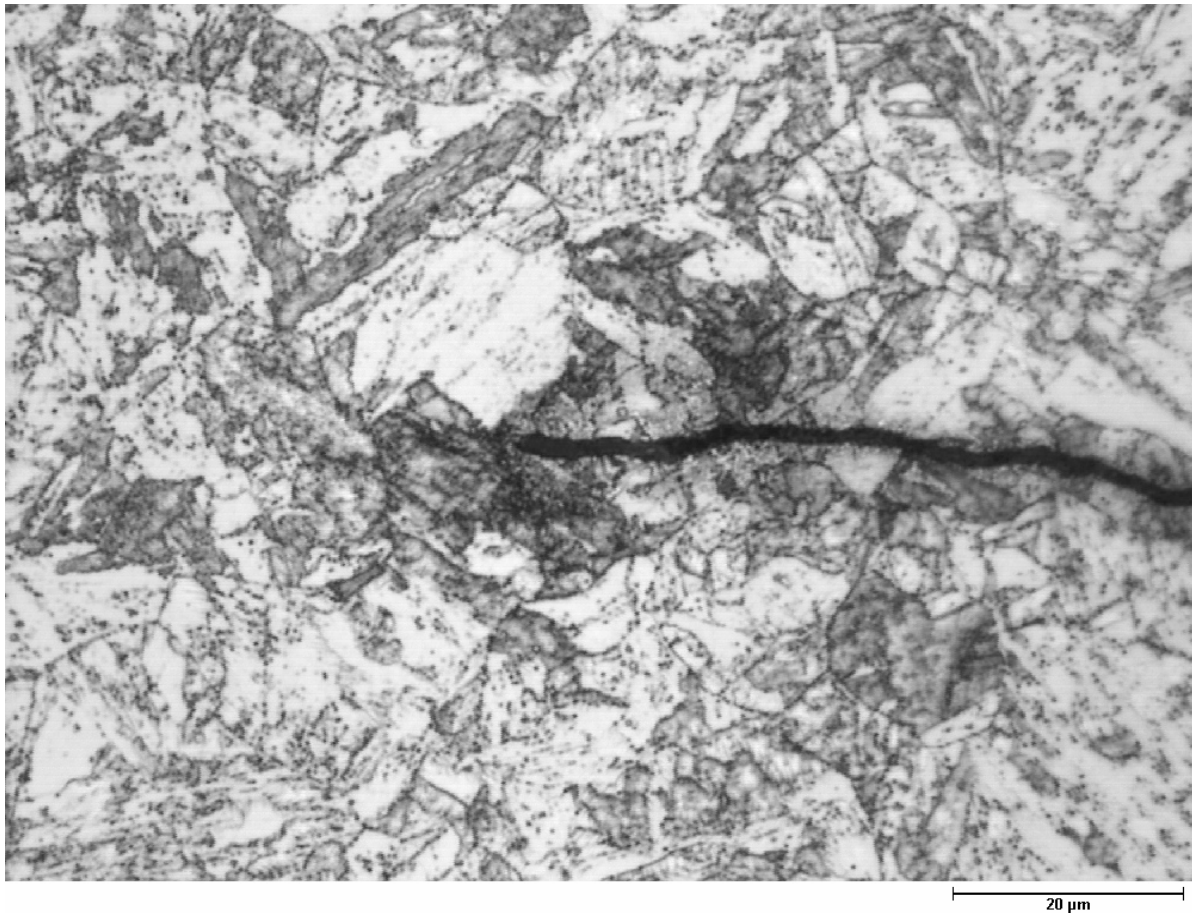
Figure 5   Light microscopy image showing exemplary the transcrystalline fatigue crack growth observed